# Supporting Information

## Basta et al. 10.1073/pnas.1321936111

### SI Materials and Methods

**Expression and Purification of the *Escherichia coli* Mechanosensitive Channel of Small Conductance.** *E. coli* mechanosensitive channel of small conductance (MscS) constructs were cloned into pET expression vectors (Novagen). The main construct consisted of an N-terminal His tag–*E. coli* MscS subcloned into the pET28b vector (1). Other constructs subcloned included an N-terminal 6× His tag–*E. coli* MscS–C-terminal FLAG tag and N-terminal 6× His tag–*E. coli* MscS–C-terminal GFP. Vectors were transformed into BL21 Gold [DE3] expression cells (Stratagene) for protein expression. Large-scale expressions were performed using a 60-L fermentor and Terrific Broth (TB) containing 0.4% glycerol. A 1-L starter culture in TB was used to inoculate the fermentor and allowed to grow for 4–5 h at 37 °C. When the cell density was greater than OD = 3 at 660 nm, the cells were induced by the addition of 1 mM isopropyl β-D-1-thiogalactopyranoside for 1 h. Cells were concentrated from 60 L to 6 L in 45 min using a cell harvester. Each growth produced ∼740 g wet cell mass.

For each MscS purification, 50 g cells were resuspended into 500 mL solubilization buffer [20 mM Tris·HCl (pH 7.5), 20 mM NaCl, 30 mM imidazole, 4 mM $MgCl_2$, DNase, lysozyme, protease inhibitor tablet EDTA-Free (Roche), and 1% Fos-Choline 14] and cells were lysed by passing through a microfluidizer for a minimum of four passes. The sample was then centrifuged at 14,000 rpm (30,000 × *g*; JA-14, Beckman) for 1 h at 4 °C to remove cellular debris. The supernatant was collected and directly loaded onto a nickel affinity column (3 × 5-mL HisTrap columns connected in serial). The column was then washed with 135 mL wash buffer [20 mM Tris·HCl (pH 7.5), 95 mM imidazole, 430 mM NaCl, 0.05% Fos-Choline 14, 100 μM PMSF, 10% (vol/vol) glycerol, protease inhibitor tablet]. MscS was eluted using 70 mL elution buffer [20 mM Tris·HCl (pH 7.5), 300 mM imidazole, 230 mM NaCl, 0.05% Fos-Choline 14, 100 μM PMSF, 10% glycerol, protease inhibitor tablet]. The eluted *E. coli* MscS was combined and diluted 1:5 in 25 mM Tris (pH 7.5), 0.05% Fos-Choline 14, and protease inhibitor tablet to reduce the salt concentration. Samples were then concentrated to 10–15 mL using an anion exchange column and further concentrated to 2 mL using a 100-kDa molecular weight cutoff Amicon Ultra 15 concentrator (Millipore). The protein was then loaded onto a Sephacryl S300 26/60 gel filtration column. The average amount obtained from 50 g of cells was 6.7 mg of *E. coli* MscS.

**Membrane Protein Polyhedral Nanoparticle Formation by Dialysis.** Purified proteins were used to form membrane protein polyhedral nanoparticles (MPPNs) at a concentration of 1 mg/mL. Lipids were dissolved at 5 mg/mL in 1% CHAPS and used at varying concentrations (0.01–1 mg/mL). During optimization, different buffers were used: 50 mM phosphate (pH 5.8–8.0), 50 mM Tris (pH 6.8–9.0), or 50 mM McIlvain's buffers (pH 4–8). During optimization, the MPPN solution contained 25–250 mM NaCl and 1 mM sodium azide. The typical optimized MPPN solution contained 50 mM Tris (pH 7.0), 100 mM NaCl, 1 mM sodium azide, 1 mg/mL protein, and 0.1 mg/mL lipid in 50 μL volume. Samples were dialyzed against buffer matching the sample buffer, but omitting protein and lipid, at a 1:5,000 ratio for 7–14 d at 17 °C without stirring in 8–50 kDa (15 kDa after optimization) micro Tube-O-Dialyzer units (Biosciences). A qualitative assessment of experimental conditions affecting MPPN formation is summarized in Table S1.

**Determination of Total Phosphorus.** Total phosphorus in samples was determined as previously described (2, 3). Briefly, 225 μL 8.9 M sulfuric acid was added to dried samples/standards and heated for 25 min at 200–215 °C. Linear dilutions of 0.5 mg/mL phosphatidylcholine (PC14) in 1% CHAPS were used as standards. Samples were cooled down to room temperature and 75 μL $H_2O_2$ was added followed by heating for an additional 30 min; 1.95 mL deionized $H_2O$, 250 μL 2.5% ammonium molybdate tetrahydrate and 250 μL 10% ascorbic acid were added into samples previously cooled to room temperature. The samples were incubated at 100 °C for 7 min and after cooling to room temperature the absorbance was measured at 820 nm. The results are summarized in Fig. S1.

**Dynamic Light Scattering.** Dynamic light scattering (DLS) experiments were performed on protein solutions and MPPN solutions as prepared above and the data analyzed using DynaPro Dynamics Version 6.3.40 software. No dilutions or buffer exchanges were performed before DLS analysis.

**Electron Microscopy and 3D Particle Averaging.** ***Negative stain.*** Suspensions of MPPNs (4 μL volume) were applied to formvar-coated, carbon-stabilized, glow-discharged 300 mesh electron microscopy grids. After 30 s, the grid was blotted with filter paper and a drop of 2% uranyl acetate was applied and blotted. Grids were examined using a Tecnai CM100 electron microscope operating at 80 kV and images were recorded using an AMT V600 camera (Advanced Microscopy Techniques Corp.). ***Electron cryotomography and PEET averaging.*** MPPNs (4 μL volume) were adsorbed to Holey Carbon Grids (Quantifoil) for 30 s, and an additional 1 μL concentrated 10 nm colloidal gold (British Biocell) was added to the grid as a source of fiducial markers for subsequent alignment of tomograms. Grids with sample were blotted and plunge frozen into a mixture of liquid propane and ethane (63:37) using a Vitrobot Mark IV (FEI). Frozen grids were transferred under liquid nitrogen to a Gatan-626 cryoholder (Gatan, Inc.) and data were collected using an FEI Tecnai F20 microscopeoperating at 200 kV with a Gatan Ultrascan 895 CCD camera. Tilt series were collected between −60° and +60° at 1.5° increments using automated acquisition software SerialEM (4). The total electron dose for each series was $<100\ e^-$ per $A^2$. Tomograms were reconstructed from tilt series data by weighted back-projection using IMOD software package (http://bio3d.colorado.edu/imod) (5). Subvolumes for 162 particles were selected from eight single-tilt tomograms by placing a model point at the center of each MPPN and were input to the Particle Estimation for Electron Tomography program (PEET) (http://bio3d.colorado.edu/PEET) (6) for alignment and averaging. A single particle from the tomogram was chosen as a reference, and the optimal alignment of each particle to the reference was found. Subsequent iterations refined the optimal alignment found in the previous iteration by aligning to a new reference generated from some of the particles aligned on the previous iteration. During the particle alignment step in PEET, we observed a strong orientation bias due to the missing wedge of data that resulted in incomplete particle reconstructions. To overcome this alignment bias, we assigned random orientation values to all particles and constrained possible angular movements to achieve a more uniform distribution of orientations (Fig. S2). This strategy resulted in a much-improved density map that revealed individual molecules with a size and shape that were in good agreement to the known molecular structure of

MscS. Using the Fourier shell coefficient (FSC), the resolution of this reconstruction was estimated as ~4 nm (Fig. S3).

***Single-particle electron cryomicroscopy.*** Samples were prepared similarly as for electron cryotomography. Data were collected at a temperature of 77 K on a Tecnai F30 electron microscope in low-dose mode at a magnification of 59,000×. Exposures were 1 s with a total electron dose of 12 $e^-$ per $Å^2$ and were recorded on Kodak SO-163 film. Images were scanned using a Zeiss SCAI film scanner with a 7-μm-pixel size corresponding to 1.186 Å per pixel. Images were then compressed threefold to achieve a final pixel size of 3.56 Å for the 3D reconstruction. Individual particles were selected manually from a total of 55 images having defocus values from 1.7 to 3.4 μm. A 3D reconstruction was performed using the Electron Micrograph Analysis 2 (EMAN2) software package (http://blake.bcm.tmc.edu/EMAN2) (7). Briefly, individual images were contrast transfer function (CTF)-corrected for initial particle classification and then the CTF was subsequently refined for particle sums from each image. A total of 4,564 particles were used for the 3D reconstruction with imposed octahedral symmetry. The final map had a resolution of 8.7 Å based on a 3σ-FSC cutoff of 0.14 (Fig. S5).

***Analysis of MPPN polyhedral symmetry.*** The polyhedral configuration of the MscS MPPN was determined by a brute-force fit of the vertices of convex regular polyhedra onto the centroids of the cytoplasmic cavity of MscS in the MPPN tomogram map. A total of 18 MscS heptamers [Protein Data Bank (PDB) ID code 2OAU] were manually docked (8) into the MPPN tomographic map, and rigid-body refinement was performed using MolRep (9). Because the MscS cytoplasmic cavity is one of the most distinguishing features in the tomogram map, the centroids of the MscS cytoplasmic cavities were chosen as vertices of the MPPN. A program was written to automate the brute-force least-square minimization fitting of the MPPN vertices with the vertices of convex regular polyhedra by optimizing seven different parameters: size, Euler angles, and center of a polyhedron. The minimization function is defined as the sum of the distance squared between a closest MPPN vertex to a fitted polyhedron vertex summed over all MPPN vertex points. One hundred thirty-two polyhedron vertex configurations were fitted from the online Encyclopedia of Polyhedra (10): 5 Platonic solids, 13 Archimedean solids (with two chiral pairs), 13 Catalan solids (with two chiral pairs), and 92 Johnson solids (with five chiral pairs); of these, the snub cuboctahedron (dextro) arrangement gave the best agreement between the observed and calculated positions (Table S2).

***Sevenfold averaging of single-particle MPPN reconstruction.*** The fit of MscS (PDB 2OAU) was rigid body refined with REFMAC (11) against structure factors calculated by Fourier inversion of the single-particle reconstruction. Noncrystallographic symmetry operators for the sevenfold molecular symmetry were obtained from the refined coordinates using the algorithm of Kabsch (12). These operators were used to sevenfold average the electron density within an MscS heptamer from the single-particle reconstruction, using the Collaborative Computational Project No. 4 crystallographic programming suite (13).

***Microfluidic device fabrication.*** The fabrication of the microfluidic device was based on the soft lithography method that patterned the SU-8 mold on a silicon wafer (14). Liquid polydimethylsiloxane (PDMS) was poured into the SU-8 mold. After thermal cure, the PDMS microstructure defined by the SU-8 was fabricated as shown in Fig. S5. The PDMS microstructure was bonded to a glass slide after oxygen plasma surface treatment as previously described (15). This method is commonly used in fabricating microfluidic devices.


1. Bass RB, Strop P, Barclay M, Rees DC (2002) Crystal structure of *Escherichia coli* MscS, a voltage-modulated and mechanosensitive channel. *Science* 298(5598):1582–1587.
2. Chen PS, Toribara TY, Warner H (1956) Microdetermination of phosphorus. *Anal Chem* 28:1756–1758.
3. Fiske CH, Subbarow Y (1925) The colorimetric determination of phosphorus. *J Biol Chem* 66:375–400.
4. Mastronarde DN (2005) Automated electron microscope tomography using robust prediction of specimen movements. *J Struct Biol* 152(1):36–51.
5. Kremer JR, Mastronarde DN, McIntosh JR (1996) Computer visualization of three-dimensional image data using IMOD. *J Struct Biol* 116(1):71–76.
6. Nicastro D, et al. (2006) The molecular architecture of axonemes revealed by cryoelectron tomography. *Science* 313(5789):944–948.
7. Ludtke SJ, Baldwin PR, Chiu W (1999) EMAN: Semiautomated software for high-resolution single-particle reconstructions. *J Struct Biol* 128(1):82–97.
8. Emsley P, Lohkamp B, Scott WG, Cowtan K (2010) Features and development of Coot. *Acta Crystallogr D Biol Crystallogr* 66(Pt 4):486–501.
9. Vagin A, Teplyakov A (2010) Molecular replacement with MOLREP. *Acta Crystallogr D Biol Crystallogr* 66(Pt 1):22–25.
10. Hart GW (2000) The Encyclopedia of Polyhedra. Available at www.georgehart.com/virtual-polyhedra/vp.html. Accessed December 17, 2013.
11. Murshudov GN, Vagin AA, Dodson EJ (1997) Refinement of macromolecular structures by the maximum-likelihood method. *Acta Crystallogr D Biol Crystallogr* 53(Pt 3):240–255.
12. Kabsch W (1976) A solution for the best rotation to relate two sets of vectors. *Acta Crystallogr A* 32:922–923.
13. Collaborative Computational Project, Number 4 (1994) The CCP4 suite: Programs for protein crystallography. *Acta Crystallogr D Biol Crystallogr* 50(Pt 5):760–763.
14. Unger MA, Chou HP, Thorsen T, Scherer A, Quake SR (2000) Monolithic microfabricated valves and pumps by multilayer soft lithography. *Science* 288 (5463):113–116.
15. Cha J, et al. (2006) A highly efficient 3D micromixer using soft PDMS bonding. *J Micromech Microeng* 16:1778–1782.

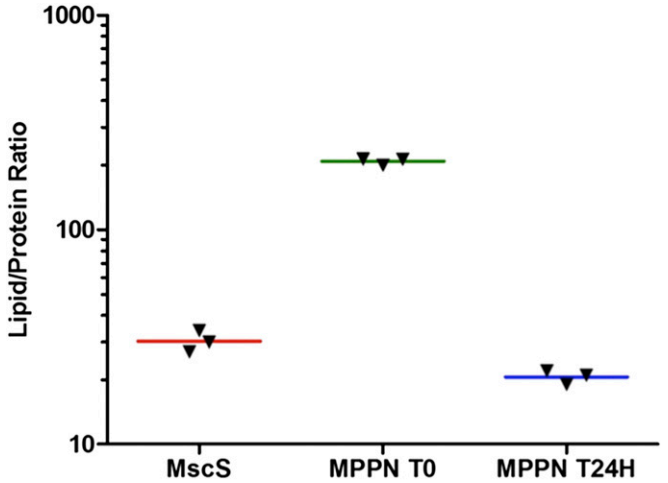


**Fig. S1.** Lipid:protein ratios as measured by combined protein bicinchoninic acid assay and phosphorous analysis for three separate dialysis trials. MscS, starting protein ratio; MPPN T0, sample at the beginning of dialysis; MPPN T24H, sample at completion of dialysis at 24 h.

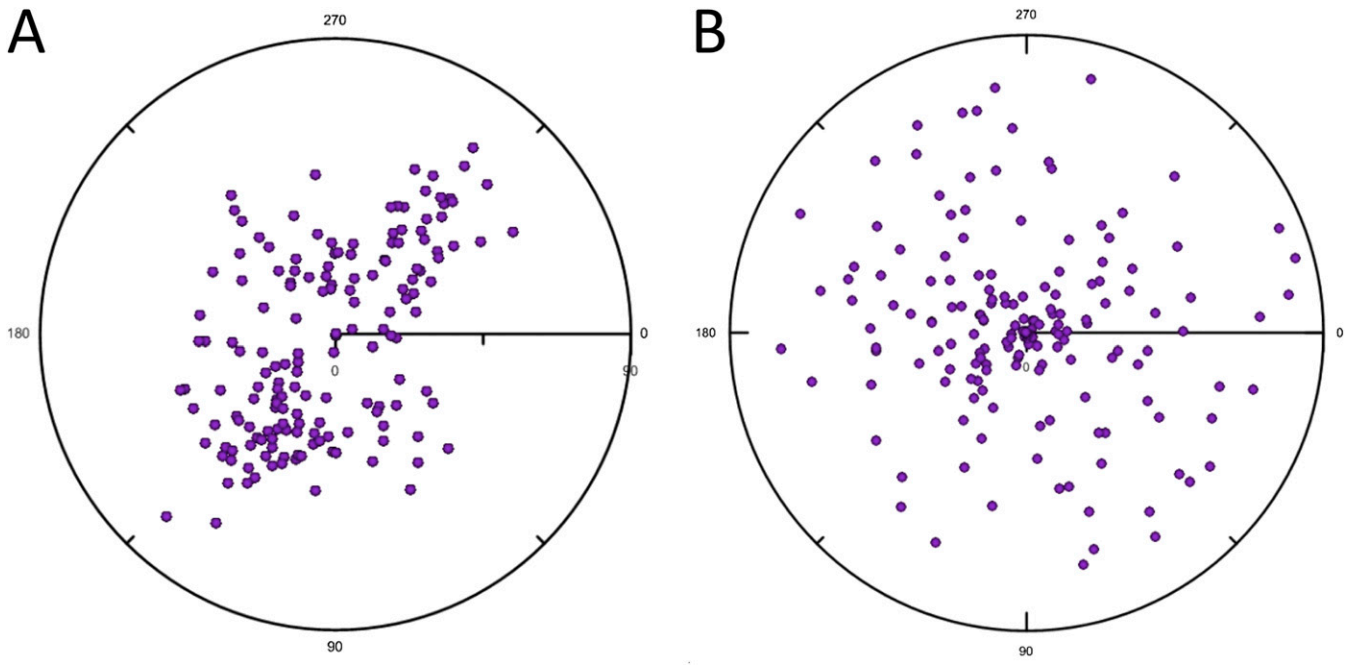


**Fig. S2.** (*A*) Polar plot of final Euler angles without initial randomization. (*B*) Polar plot of final Euler angles after initial randomization before alignment. The randomization of the initial Euler angles resulted in a more uniform distribution of final alignment angles compensating for the missing wedge bias.

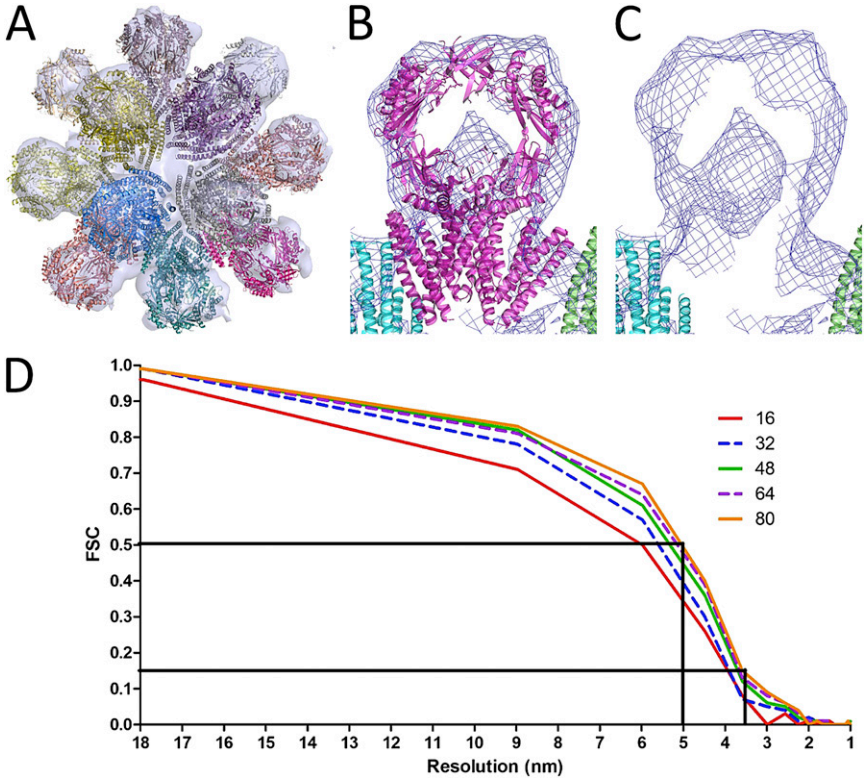


**Fig. S3.** PEET image reconstruction following application of 432 symmetry on the cryotomography map. (*A*) Fit of individual MscS molecules to the symmetrized map as in Fig. 2*C*. (*B*) Close-up of the fit of one MscS molecule to the averaged density, showing the clear presence of the cytoplasmic chamber of MscS in the density map. (*C*) As in *B* omitting the central MscS molecule. (*D*) FSC for the PEET reconstruction. The FSC shows the progressive improvement in resolution with the addition of more particles, with the number of particles (*Inset*) represented by different colored lines. Using a FSC cutoff of 0.5 the resolution is estimated to be ~5 nm. Using a 3σ FSC cutoff of 0.14 the resolution is estimated to be ~3.5 nm. The actual map appears to have at least a 4-nm resolution as one can clearly resolve the cytoplasmic cavity of MscS which has an inner radius of 2.5 nm and an outer radius of 4 nm.

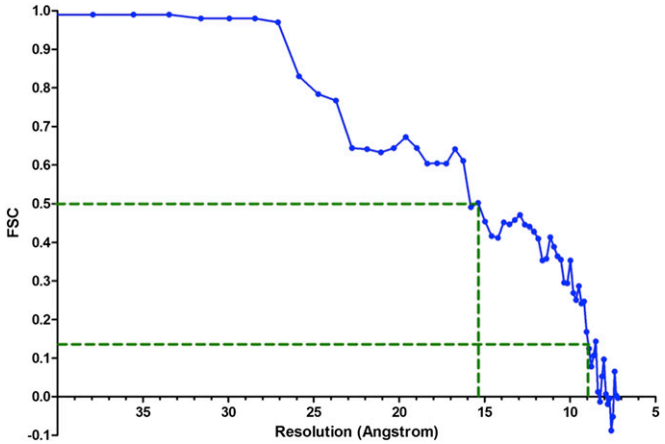


**Fig. S4.** FSC (blue dots) for the single-particle reconstruction. Using an FSC cutoff of 0.5 the resolution is estimated to be 15.3 Å. Using a 3σ FSC cutoff of 0.14 the resolution is estimated to be 8.9 Å. FSC calculated using e2refine_evenodd in EMAN2.

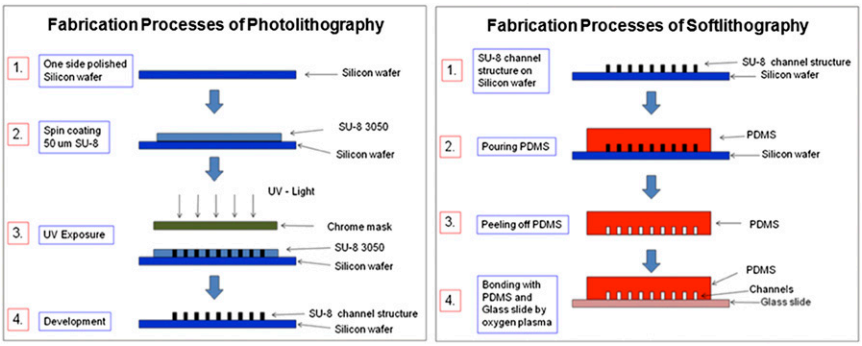


**Fig. S5.** Fabrication processes of photolithography. The numbers in the figure correspond to the following: (*Left*) 1. preparation of one-side polished silicon wafer; 2. spin coating of SU-8 on the silicon wafer; 3. UV exposure; 4. development for removing un–cross-linked SU-8. Fabrication processes of soft lithography; and (*Right*) 1. fabrication of SU-8 channel structures on silicon wafer; 2. molding of PDMS structure on the silicon wafer without bubbles. 3. removal of the PDMS structure from the silicon wafer; 4. bonding PDMS structure and glass slide by using oxygen plasma-based surface treatment.

**Table S1. Qualitative assessment of experimental conditions affecting MPPN formation**

| | | pH | | |
|---|---|---|---|---|
| Lipid | Protein isoelectric point | 5 | 7 | 9 |
| PC14 | 8.9 | + | +++ | ++ |
| PS14 | 8.9 | ++ | ++ | + |
| PC14 | 6.7 | – | +/– | +/– |
| PS14 | 6.7 | – | +/– | +/– |
| PC12 | 8.9 | + | ++ | ++ |
| PC16 | 8.9 | – | + | – |

+, ++, or +++, favorable conditions for MPPN formation (where +++ represents the best conditions identified in this study); +/– , partial MPPN formation; – no MPPN formation. Four variables influencing MPPN formation were surveyed: (*i*) lipid headgroup/charge with PC14 and PS14 designating the zwitterionic phosphatidycholine and anionic phosphatidylserine headgroups, respectively (both with fatty acid alkyl chains containing 14 carbons); (*ii*) alkyl chain lengths, with PC12 and PC16 designating phosphatidylcholine with fatty acid alkyl chains containing 12 and 16 carbons, respectively; (*iii*) protein charge as reflected by the calculated isoelectric point (IP), with IP 8.9 and IP 6.7 representing the more positively charged His-tag and the more negatively charged Flag-tag MscS constructs, respectively; and (*iv*) solution pH. While all parameters influenced MPPN formation, the best results were found with PC14 and His-tagged MscS at pH 7. Theoretical pIs were calculated using the ProtPram tool from the ExPasy Proteomics server (http://ca.expasy.org/tools/protparam.html).

**Table S2. Top 25 polyhedron vertex fit solutions**

| Type | Polyhedron | Fit error, Å$^2$* | rmsd, Å | rmsd/edge length† |
|---|---|---|---|---|
| Archimedean solid | Snub cuboctahedron (dextro) | 5,958.40 | 18.19 | 0.17 |
| Catalan solid | Pentagonal icositetrahedron (dextro) | 8,926.76 | 22.27 | 0.21 |
| Archimedean solid | Snub cuboctahedron (levo) | 9,299.95 | 22.73 | 0.21 |
| Johnson solid | Gyroelongated square bicupola (J45) chiral 2 | 9,569.93 | 23.06 | 0.21 |
| Johnson solid | Gyroelongated square bicupola (J45) chiral 1 | 9,577.13 | 23.07 | 0.21 |
| Catalan solid | Trapezoidal icositetrahedron | 10,048.62 | 23.63 | 0.22 |
| Catalan solid | Disdyakisdodecahedron | 10,454.44 | 24.10 | 0.22 |
| Catalan solid | Pentagonal icositetrahedron (levo) | 11,958.47 | 25.78 | 0.24 |
| Johnson solid | Elongated square gyrobicupola (J37) | 12,160.74 | 25.99 | 0.24 |
| Catalan solid | Disdyakistriacontahedron | 12,824.18 | 26.69 | 0.25 |
| Catalan solid | Trapezoidal hexecontahedron | 13,347.44 | 27.23 | 0.25 |
| Catalan solid | Pentakisdodecahedron | 13,632.20 | 27.52 | 0.26 |
| Johnson solid | Elongated pentagonal gyrocupolarotunda (J41) | 14,266.88 | 28.15 | 0.26 |
| Archimedean solid | Rhombicuboctahedron | 14,330.15 | 28.22 | 0.26 |
| Catalan solid | Rhombic triacontahedron | 14,432.81 | 28.32 | 0.26 |
| Johnson solid | Elongated pentagonal orthocupolarotunda (J40) | 14,784.11 | 28.66 | 0.27 |
| Catalan solid | Pentagonal hexecontahedron | 15,118.90 | 28.98 | 0.27 |
| Johnson solid | Gyroelongated pentagonal cupolarotunda (J47) chiral 2 | 15,134.68 | 29.00 | 0.27 |
| Catalan solid | Triakisicosahedron | 15,431.34 | 29.28 | 0.27 |
| Johnson solid | Elongated pentagonal gyrobicupola (J39) | 15,460.15 | 29.31 | 0.27 |
| Johnson solid | Pentagonal orthobirotunda (J34) | 15,994.24 | 29.81 | 0.28 |
| Johnson solid | Gyroelongated pentagonal cupolarotunda (J47) chiral 1 | 16,442.82 | 30.22 | 0.28 |
| Johnson solid | Elongated pentagonal orthobirotunda (J42) | 17,585.34 | 31.26 | 0.29 |
| Johnson solid | Gyroelongated pentagonal birotunda (J48) chiral 2 | 17,690.01 | 31.35 | 0.29 |
| Johnson solid | Gyroelongated pentagonal birotunda (J48) chiral 1 | 17,789.99 | 31.44 | 0.29 |

*Fit error is the sum of the distance squared between a closest MPPN vertex to a fitted polyhedron vertex summed over the 18 MscS molecules defining the observed vertex points.

†rmsd divided by the closest edge length of MPPN vertices indicates the overall goodness of a solution.